

# Multifunctional Chiral Silanol Ligands for Enantioselective Catalysis

Yun-Pu Chang, Kevin Blanco-Herrero, Turki M. Alturaifi, James C. Fettinger, Peng Liu, and Annaliese K. Franz\*

[a] Y.-P. Chang, K. Blanco-Herrero, Dr. J. C. Fettinger, Prof. A. K. Franz

Department of Chemistry, University of California–Davis

One Shields Avenue, Davis, CA 95616, (USA)

E-mail: [akfranz@ucdavis.edu](mailto:akfranz@ucdavis.edu)

T. M. Alturaifi, Prof. P. Liu

Department of Chemistry, University of Pittsburgh

219 Parkman Avenue, Pittsburgh, PA 15260, (USA)

E-mail: [penqliu@pitt.edu](mailto:penqliu@pitt.edu)

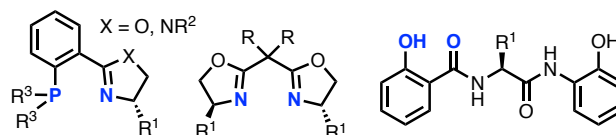
**Abstract:** We report transition metal catalysis using novel chiral metal-chelating ligands featuring a silanol coordinating group and peptide-like aminoamide scaffold. The catalytic properties of the silanol ligands are demonstrated through an enantioselective Cu-catalyzed N–H insertion affording unnatural amino acid derivatives in high selectivity. Our investigations into the silanol coordination mode include DFT calculations, ligand analogs, NMR and X-ray structure analyses, which support the formation of an H-bond stabilized silanol-chelating copper carbenoid complex. A  $\pi$ - $\pi$  stacking interaction revealed by DFT calculations is proposed to enable selectivity for aryl diazoacetate substrates, overcoming the traditional limitations of using these substrates.

Enantioselective catalysis is widely considered as the most efficient method to prepare enantioenriched compounds.<sup>[1–3]</sup> In metal-catalyzed reactions, chiral ligands are utilized to control reactivity and stereoselectivity. Considerable efforts have been made to design and synthesize classes of ligands for a variety of chemical transformations.<sup>[4,5]</sup> The heteroatoms serving as coordinating sites are key to chiral ligand design principles<sup>[6,7]</sup>, allowing for the stereocontrol and tuning of reactivity. Common metal-coordinating groups include phosphines,<sup>[8–12]</sup> phosphites,<sup>[13–15]</sup> amines,<sup>[8,16]</sup> imines,<sup>[17,18]</sup> and alcohols<sup>[16–21]</sup> (Figure 1A).<sup>[7]</sup> Silicon has been incorporated in the backbone of a chiral ligand scaffold,<sup>[22–27]</sup> and the hydrosilane introduced as a coordinating group for catalysis,<sup>[28–33]</sup> yet, there are no examples of silanols in metal-coordinating ligands for transition-metal catalyzed enantioselective synthesis.

The silanol (Si–OH) group provides an opportunity to design ligands with new coordination modes for enhanced activity and stereoselectivity in asymmetric catalysis. Metal siloxides are more Lewis acidic than metal alkoxides due to back-bonding interactions ( $O_{lp} \rightarrow \sigma^*_{Si-O}$ )<sup>[34,35]</sup> and the angle-dependent donor capacity of metal siloxides may bring balanced reactivity to catalytic cycles.<sup>[36,37]</sup> Furthermore, longer Si–O bonds can contribute to improved steric modulation and selectivity. Achiral silanols have been previously utilized as ancillary ligands for a variety of metal-catalyzed transformations<sup>[38]</sup> such as alkyne metathesis,<sup>[37,39,40]</sup> Pd-catalyzed cross-coupling<sup>[41–44]</sup> and ortho-metalation,<sup>[45–49]</sup> Strohmann has reported chiral zinc(II)-silanoates,<sup>[50]</sup> including a stereogenic-silicon silanoate,<sup>[51]</sup> although no catalytic activity was documented. A notable example

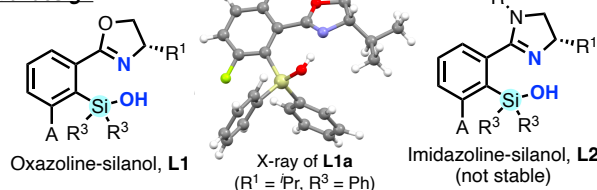
of a ferrocene-based chiral organosilanol ligand has been reported for an asymmetric phenyl-transfer reaction to substituted benzaldehydes with stoichiometric zinc reagents.<sup>[52]</sup> Building upon catalytic features observed in achiral metal-siloxide examples, we have developed a novel modular multifunctional chiral ligand scaffold possessing silanol and amide coordination sites, enhanced by intramolecular H-bonding stabilization between the amino and silanol groups (Figure 1B). The subsequent use of these ligands in N–H insertion reactions represents the first example of a silanol in a chelating ligand for a catalytic enantioselective transformation.

## (A) Examples of chiral ligands with common coordinating groups



## (B) This work: chiral ligands featuring a silanol coordinating group

### Initial design



### Discovery of the aminoamide-silanol ligand, L3

SiOH, amide, and NHAr are three key components in ligand;

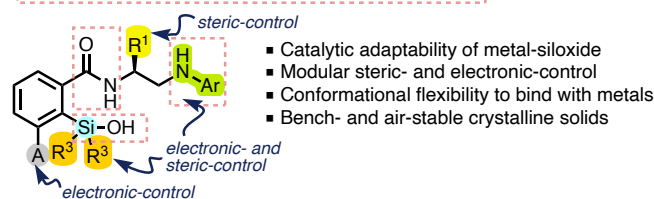


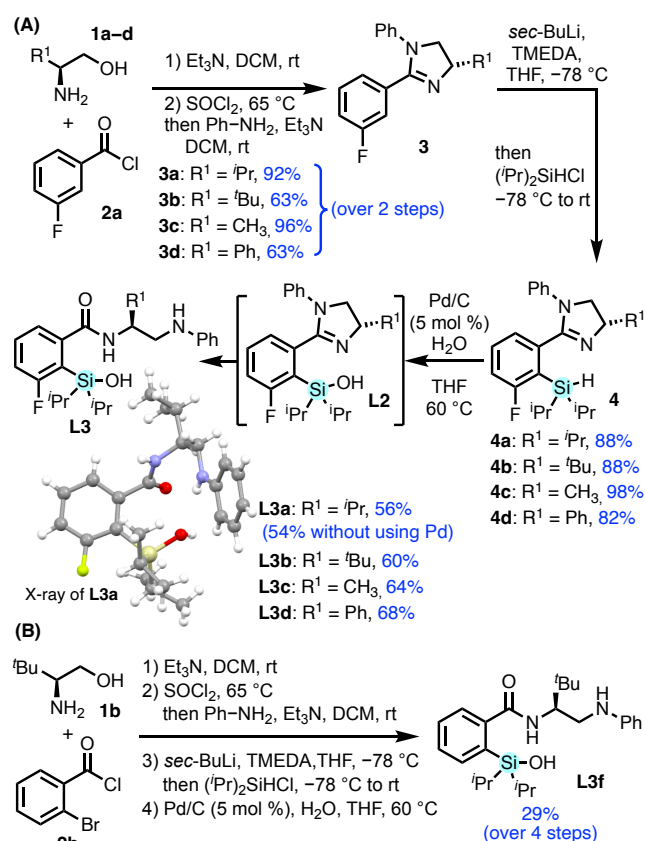
**Figure 1.** (A) Common coordinating groups in asymmetric catalysis. (B) This work: silanol coordinating group in chiral ligand design.

At the start of our investigation, we envisioned incorporating silanol chelating groups onto tunable chiral oxazoline (**L1**) and imidazoline (**L2**) scaffolds, which are common ligands employed in a variety of enantioselective transformations (Figure 1B).<sup>[4,53–55]</sup> Initial results with **L1** showed poor reactivity and selectivity in several test reactions. Upon synthesis and evaluation of

imidazoline-silanol **L2** with the goal to enhance enantioselectivity,<sup>[11]</sup> we discovered a novel aminoamide ligand **L3** formed via silanol-facilitated ring-opening of the imidazoline ring (see Supporting Information Section III) (Figure 1B).

Following this discovery, we prepared a collection of aminoamide silanol ligands (**L3**) through an efficient modular synthetic sequence (Scheme 1). The general synthetic procedure utilizes an amide coupling and cyclization to form imidazoline **3**, followed by *ortho*-lithiation<sup>[56]</sup> and addition of a chlorosilane to afford silane **4**. Silanols **L3** were obtained upon hydrolysis of silane **4** using catalytic Pd/C with H<sub>2</sub>O.<sup>[57]</sup> However we observed that the imidazoline promotes formation of silanol **L3a** without requiring a Pd/C catalyst (see Supporting Information Section III). The route from inexpensive starting materials is scalable up to 1.5 grams. All of the aminoamide silanol products are air-stable, crystalline white solids.<sup>[58]</sup> Synthesis via silane **4** provides unique access to **L3**; hydrolysis via the corresponding silyl chloride or direct silylation of the amide were not successful (see Supporting Information Section V).

**Scheme 1.** Synthesis of chiral aminoamide silanol ligands (**L3**).



With the goal to demonstrate the silanol as a novel coordinating group in ligand design, an N-H insertion reaction serves as a model reaction to highlight our preliminary discoveries. The catalytic properties of aminoamide-silanol ligands **L3** were explored via an enantioselective N-H insertion of  $\alpha$ -phenyl- $\alpha$ -diazoester (**5a**) with aniline (Figure 2).<sup>[59]</sup> Enantioselective N-H insertions have proven to be a highly efficient way to form C-N bonds and can be used for the synthesis of unnatural chiral amino acids.<sup>[59-69]</sup> Previous enantioselective N-H insertions have utilized

rigid spirobox,<sup>[59,60,68]</sup> bipyridine,<sup>[67]</sup> and *N,N*-dioxide<sup>[66]</sup> ligands or catalyst systems combining chiral H-bonding catalysts with copper.<sup>[63,64]</sup> Notably, the silanol ligands can be used in the N-H insertion reaction without the use of a glovebox while maintaining high enantioselectivity. While initial experiments utilizing oxazoline-silanol **L1** resulted in poor enantioselectivity, a remarkable improvement was observed using silanol **L3a**, highlighting the importance of the aminoamide backbone for enantioselectivity. Following initial success with **L3a**, we focused on optimizing the reaction conditions including [Cu] source, solvent, temperature and reaction concentration (see Table S3). The absence of copper resulted in no reaction, and addition of NaBAR<sup>F</sup> is essential for this reaction to proceed selectively. A control experiment without **L3a** confirms that the ligand is critical for inducing enantioselectivity. Comparison using non-silanol analogs **L4** and **L5**, where the silanol is replaced with a trimethylsilyl group (**L4**)<sup>[70]</sup> or a COH (**L5**), resulted in a complete loss of enantioselectivity, albeit a background rate is still observed from the unchelated copper catalyst. These analogs support that silanol coordination is crucial for control of enantioselectivity (See Table S5 for more control experiments).

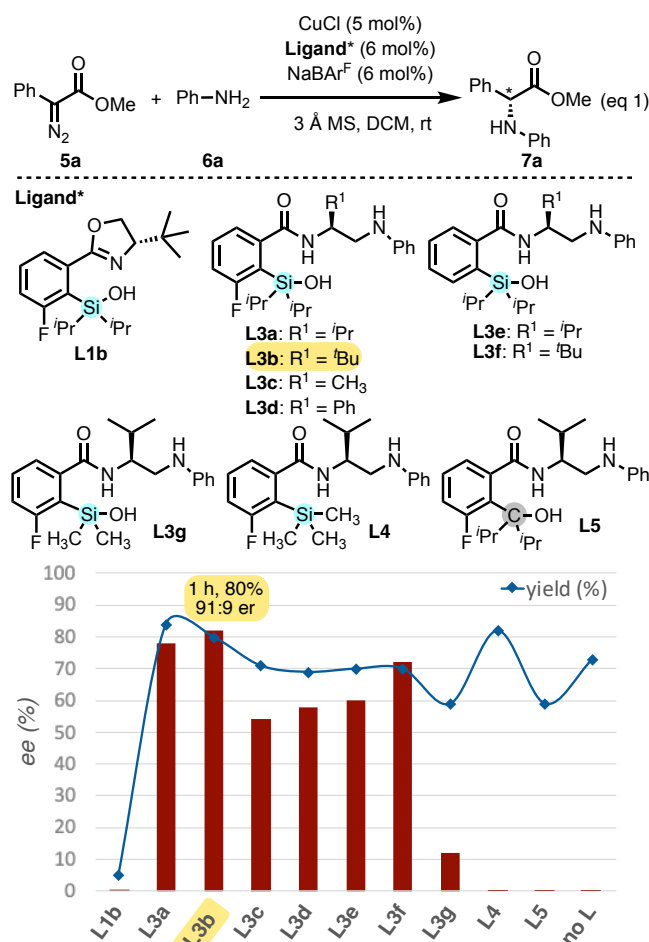


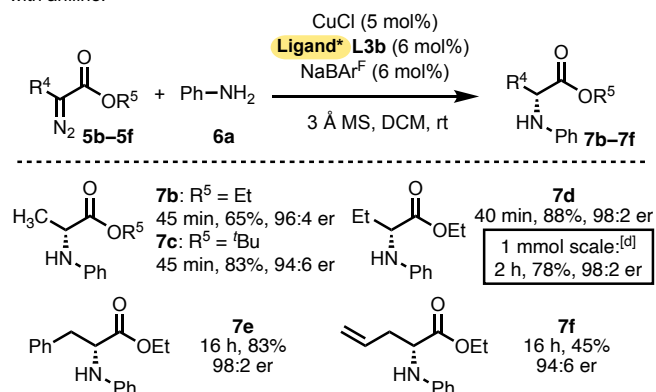
**Figure 2.** Ligand optimization for the enantioselective N-H Insertion of  $\alpha$ -phenyl- $\alpha$ -diazoesters with aniline (see SI for raw data). Standard reaction conditions: **5a** and **6a** (0.2 mmol, 1.0 equiv each), CuCl (5 mol %), NaBAR<sup>F</sup> (6 mol %), ligand (6 mol %), and spherical 3Å mol sieves (50 mg) in DCM (0.05 M) at room temperature. For **L3**-**L5** and no L, reactions proceeded with full consumption of **5a** in 1 h; for **L3c** in 2 h. Reactions with **L1b** required 16 h for

74% (60:40 er); however, data for the 1 h time point for **L1b** is graphed for direct comparison. Yield determined using NMR spectroscopy with Ph-TMS as internal standard. Enantiomeric excess (ee %) determined using CSP-HPLC analysis with a Chiralpak OD-H column. **L1** produced the opposite enantiomer.

To evaluate the modular ligand components we synthesized a series of silanol ligands (**L3b-g**) (Figure 2).<sup>[71]</sup> The enantioselectivity of the N–H insertion (**L3a-d**) is influenced by the steric groups (R<sup>1</sup>) at the chiral center; however, **L3a** and **L3b** exhibit similar performance (89:11 and 91:9 er, respectively). We evaluated the effect of the fluoride on the core aryl ring (**L3h-i**), which was originally incorporated into the backbone for synthetic purposes; in both cases, a slight reduction in enantioselectivity was observed (86:14 and 80:20 er, respectively). Ligand **L3g** with a less sterically demanding dimethylsilanol group (**L3g**) resulted in a significant decrease in enantioselectivity (89:11 vs 56:44 er).

Next we evaluated the substrate scope for the enantioselective N–H insertion reaction using our optimal silanol ligand **L3b**. The reaction proceeds in high enantioselectivity (94:6 to 98:2 er) using various alkyl diazoesters with aniline (Scheme 2). A bulky *tert*-butyl ester on the  $\alpha$ -diazopropanoate retains high selectivity (96:4 vs 94:6 er) albeit with higher yield of product (**7b**<sup>[72]</sup> and **7c**). The reaction of ethyl 2-diazobutanoate proceeds with excellent yield and enantioselectivity (**7d**, 88%, 98:2 er) and the catalytic performance was unaffected by scaling up to 1.0 mmol scale. The silanol ligand also facilitated high yields with substrates prone to  $\beta$ -H elimination, a process commonly competing with insertion to form conjugated products. Utilizing the silanol ligand mitigated this challenge, resulting in reduced side products and enhanced yields, effectively addressing issues reported previously.<sup>[68,73]</sup> For instance, when a phenyl group was positioned at the  $\beta$ -position of the diazoester, a high yield of the desired N–H insertion product (**7e**) was achieved. Additionally, the reaction tolerated an olefin (**7f**) under the reaction conditions, exhibiting high selectivity; however, a moderate yield was observed due to the inevitable competitive  $\beta$ -H elimination.<sup>[74]</sup>

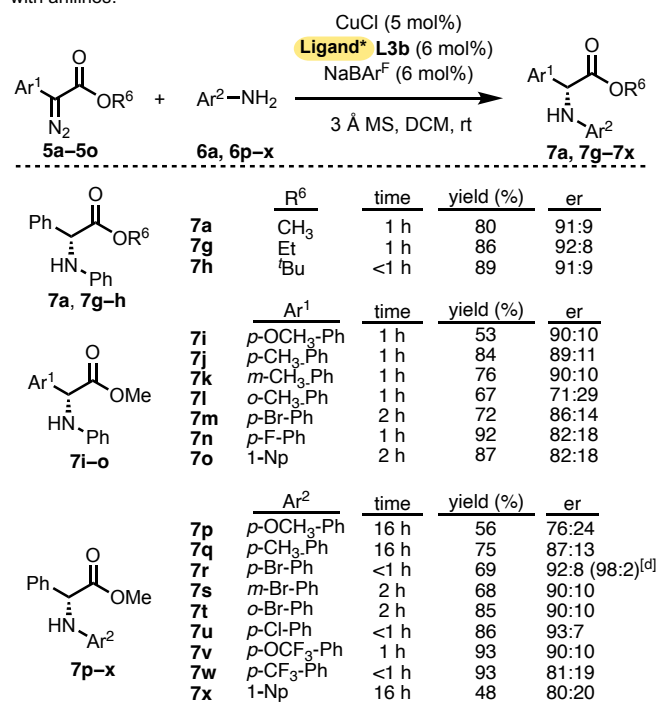
**Scheme 2.** Scope of the enantioselective N–H insertion of  $\alpha$ -alkyl- $\alpha$ -diazoesters with aniline.<sup>[a,b,c]</sup>



[a] Reactions performed under standard reaction conditions. [b] Isolated yields. [c] Determined using CSP-HPLC with a Chiralpak OD-H column. The absolute configuration was assigned as (*R*) based on HPLC data for **7b**.<sup>[59]</sup> [d] Reaction performed using 1.0 mmol of diazo **5d** and aniline **6a**.

The silanol ligand overcomes limitations related to lower enantioselectivity for N–H insertion reactions using  $\alpha$ -aryl- $\alpha$ -diazoesters resulted in lower enantioselectivity; however, employing silanol ligand **L3b** overcomes this limitation, proceeding with higher enantioselectivities for aryl substrates (Scheme 3). The enantioselectivity (91:9 er) was not affected by the steric effect on the ester (**7a**, **7g-7h**). Electronic effects at the insertion center were then investigated (**7i-7o**). The electronic profile of the aniline reactant was then explored via a Hammett analysis (Figure 3, **7p-7w**). The general mechanism of N–H insertions involve an ylide intermediate.<sup>[62,68]</sup> When the substituents stabilize the ylide, then the free ylide tends to form preferentially and the N–H insertion product is obtained with poor enantioselectivity. However, when the catalyst-associated ylide is favored, high enantioselectivity is usually observed. Based on these generally accepted hypotheses, a good correlation of the log (er) values of the products with the Hammett substituent constants<sup>[75]</sup> should be observed.<sup>[68,69]</sup> Interestingly, here a crossover point in the Hammett plot was observed (Figure 3A), indicating a change in mechanism where the strong electron-withdrawing anilines (**7q** and **7r**) start acting as achiral proton-shuttle catalysts (Figure 3B), thus leading to a decrease in enantioselectivity.

**Scheme 3.** Scope of the enantioselective N–H insertion of  $\alpha$ -aryl- $\alpha$ -diazoesters with anilines.<sup>[a,b,c]</sup>



[a] Reactions performed under standard reaction conditions. [b] Isolated yields. [c] Determined using CSP-HPLC with a Chiralpak OD-H column. The absolute configuration was assigned as (*R*) based on the HPLC data for **7h**.<sup>[76]</sup> [d] er determined after recrystallization.

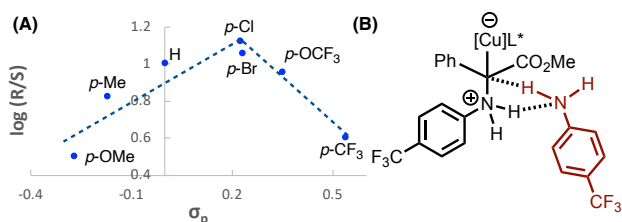


**Figure 3.** (A) Substituent effects of **7p–7w** on enantiomeric ratio. (B) Proposed  $p$ -CF<sub>3</sub>-aniline-assisted proton-transfer mechanism.

Density functional theory (DFT) calculations reveal the binding mode and conformation of ligand **L3a** with the proposed Cu–carbene complex, supporting the essential role of the silanol as a chelating group in the active complex (Figure 4).<sup>[62,63,68,69]</sup> The isopropyl was utilized in all DFT studies since both **L3a** and **L3b** exhibit comparable performance in the N–H insertion reaction. The analysis demonstrates that the most stable conformation involves both the silanol oxygen and amide carbonyl oxygen atoms coordinating relatively strongly with the copper atom, with bond distances of 2.03 Å and 2.14 Å, respectively. Additionally, intramolecular hydrogen bonding between the silanol and amino group was observed, increasing the Lewis basicity of the silanol oxygen and further stabilizing the silanol–Cu coordination. The ten-membered ring (highlighted in yellow) adopts a chair–chair–half-chair conformation<sup>[77,78]</sup> with no noticeable transannular strain and the alkyl group at the stereogenic center placed in the pseudoequatorial position. Moreover, the DFT calculations revealed a  $\pi$ – $\pi$  interaction between the N-phenyl group on the ligand and the phenyl group on the carbene, evidenced by a distance of 4.20 Å between the centroids of the two benzene rings. Traditionally, aryl diazoacetates yield low enantioselectivity in N–H insertion due to aryl stabilization of the free ylide intermediate,<sup>[62,68]</sup> while alkyl diazoacetates exhibit selectivity, potentially due to C–H  $\pi$  interactions and lower intermediate stability. We proposed silanol **L3** overcomes this traditional limitation through a  $\pi$ – $\pi$  interaction, thereby enhancing stability in the metal–ligand complex and catalyst-associated ylide.

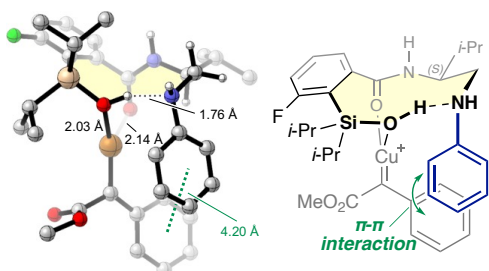
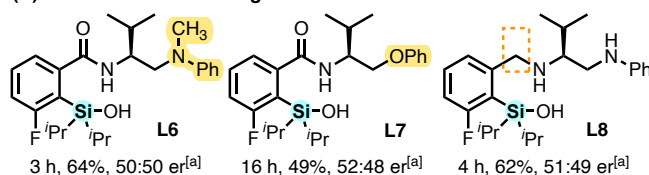


**Figure 4.** The lowest energy conformer of the proposed Cu–carbene intermediate, featuring ligand **L3a** and aryl-diazoesters **5a**, as determined by DFT calculations at the M06/6-311+G(d,p)–SDD(Cu)/SMD(DCM)//B3LYP-D3/6-31G(d)–SDD(Cu) level of theory. Structures of 10 conformers located within 3 kcal/mol of the lowest-energy conformer are provided in the Supporting Information (section XI).

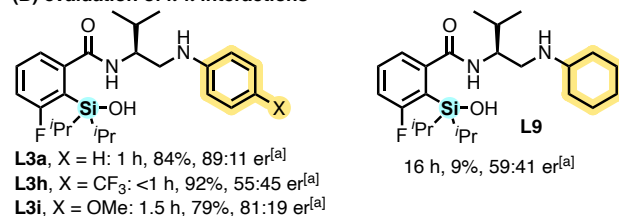
To support results of the DFT calculations, ligand analogs **L6–L8** were synthesized and evaluated for the enantioselective N–H insertion (eq 1) to investigate the H-bonding interactions within the metal–ligand complex (Figure 5A). Analogs that do not contain H-bonding interaction demonstrate a complete loss of enantioselectivity. N-methylated analog (**L6**) affords good yield

(64%) but leads in no selectivity. Similarly, the phenoxy analog (**L7**) resulted in low enantioselectivity. These observations suggest that the H-bonding interaction between the amine and silanol group is critical to promote a favorable conformation that enhances coordination of the silanol to the metal center and imparts enantioselectivity. Ligand analog **L8** without the amide carbonyl group also afforded racemic product, supporting the DFT results that both the silanol oxygen and the carbonyl oxygen play a key role for coordination in the active complex.

#### Silanol ligand analogs to investigate interactions in the active complex (A) evaluation of H-bonding interactions



#### (B) evaluation of $\pi$ – $\pi$ interactions



<sup>[a]</sup> results for the N–H insertions (eq 1)

**Figure 5.** Comparison of silanol ligand analogs in N–H insertion reaction providing insight of secondary interactions to support DFT calculations: (A) Results for N–H insertion reactions for ligands with different H-bonding capabilities (B) Results for N–H insertion reactions with ligands with capabilities for different  $\pi$ – $\pi$  interactions, supporting the effect of  $\pi$ – $\pi$  interaction observed in DFT calculations.

The  $\pi$ – $\pi$  interaction is further supported by the distinct influence of the *N*-substitution of the ligand (e.g., cyclohexyl vs phenyl) on both reactivity and selectivity (Figure 5B). A loss of enantioselectivity is observed for *N*-cyclohexyl ligand analog (**L9**, 59:41 er). The analog with a para-electron-withdrawing group on the N-aryl (**L3h**, 55:45 er) also shows a loss of enantioselectivity while the para-donating group (**L3i**) retains good enantioselectivity (81:19 er). Furthermore, when conducting the N–H insertion in aromatic solvent, a decrease in selectivity is observed (78:22 er, Table S3, entries 13–15).

Complexation studies performed using <sup>1</sup>H and <sup>29</sup>Si NMR and *in-situ* infrared spectroscopy (Figure 6) align with the silanol ligand analog studies and DFT calculations. <sup>1</sup>H NMR experiments support the secondary interactions of amide C=O binding to Cu<sup>[79–81,66]</sup> as well as H-bonding from the N–H of the amino group to both the amide C=O and the siloxide oxygen (see SI, Section VII). The <sup>1</sup>H NMR spectra revealed significant shifts of the protons on the phenyl ring attached to the amino group (Figure 6B). No evidence of oligo- or polymeric L/Cu species are observed in <sup>1</sup>H NMR binding experiments and no non-linear effect was observed. Preliminary results from *in-situ* FTIR also support H-bond stabilized silanol–metal coordination (Figure 6B, also see SI Section VII). Without NaBAR<sup>F</sup>, no obvious shifts in <sup>1</sup>H NMR spectra (Figure S9) and no selectivity in the N–H insertion was observed

(Table S4). This indicates the necessity of NaBAR<sup>F</sup> for the formation of the active Cu carbene complex.

An intermediate  $[(L3a)_2/Na \cdot (H_2O)_2]^+ [BAR^F]^-$  complex was isolated and single crystal X-ray analysis supports the formation of H-bond stabilized silanol coordination. In this intermediate, intramolecular H-bonding interactions are observed between the amino and silanol group, with additional intermolecular H-bonding between amino and amide groups. This silanol coordination observed in this sodium intermediate is consistent with the DFT calculations, highlighting the role of the silanol as a metal chelating group (Figure 6C).<sup>[82,83]</sup>

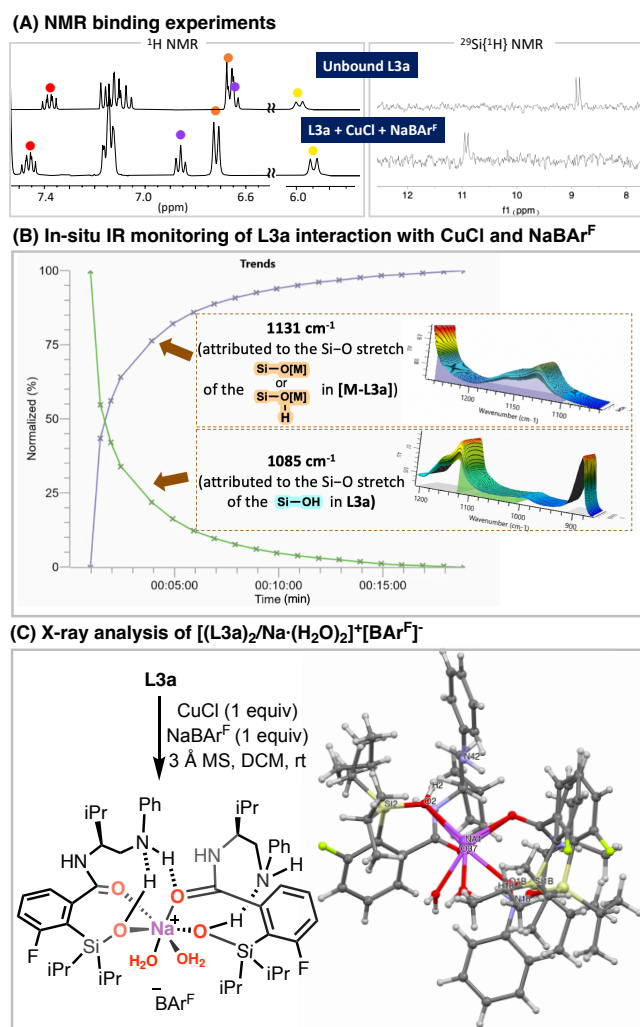


**Figure 6.** Spectroscopic studies providing insight into the H-bonding interactions within metal-silanol complex. (A) Binding experiments monitored using <sup>1</sup>H and <sup>29</sup>Si NMR spectroscopy (B) In-situ IR monitoring of L3a interaction with CuCl and NaBAR<sup>F</sup> in DCM (C) Single-crystal structure of complex  $[(L3a)_2/Na \cdot (H_2O)_2]^+ [BAR^F]^-$ . The BAR<sup>F</sup> anion has been omitted for clarity. Selected bond distances (Å), H-bonding interactions, and angles (deg): Si(2)-O(2): 1.634(4), Na(1)-O(2): 2.284(10), Na(1)-O(37): 2.441(8), O(2)-H(2)...N(42), N(18)-H(18)...O(37), ∠Si(2)-O(2)-Na(1): 133.7(2).

In conclusion, our study details the synthesis and application of new chiral aminoamide silanol ligands for enantioselective catalysis. The silanol group facilitates the formation of a H-bond stabilized silanol-copper carbenoid active complex, which is supported by DFT calculations, ligand analog studies, and X-ray

structural analysis. Our modular ligand design allows access to multiple ligand variants that demonstrate the influence of steric and electronic substituents on activity and selectivity for an N-H insertion reaction. This pioneering use of silanol ligands in transition-metal catalysis provides valuable insights for ligand design and machine learning training sets to allow a more comprehensive understanding of metal-ligand binding interactions and design features for asymmetric catalysis.

## Supporting Information

Experimental procedure, characterization data, optimization tables, mechanistic studies including binding experiments using <sup>1</sup>H NMR and *in-situ* infrared spectroscopic, results of non-linear experiment, copies of spectra, computational details, and Cartesian coordinates of all computed structures are available in the supporting information of this article. X-ray crystallographic data are available from the Cambridge Crystallographic Data Centre (CCDC).<sup>[84]</sup>

## Acknowledgements

This research was supported by the National Science Foundation (CHE-1900300 and CHE-2247505), including ReactIR instrumentation (CHE-1900300) and the dual-source X-ray diffractometer (CHE-1531193) used in this study. The Thermo Q-Exactive High-field Orbitrap used in this study is supported by National Institutes of Health (1S10OD025271-01A1). DFT calculations were carried out at the University of Pittsburgh Center for Research Computing and the Advanced Cyberinfrastructure Coordination Ecosystem: Services & Support (ACCESS) program, supported by NSF award numbers OAC-2117681, OAC-1928147, and OAC-1928224. We thank the Shaw group (UC Davis) for providing access to TLC-MS and the Olson group (UC Davis) for the use of IR spectrometer. We also thank the UC Davis NMR facility for their assistance with NMR techniques. YPC thanks the UC Davis graduate studies for 2022-23 Summer Graduate Student Researcher Award.

**Keywords:** Asymmetric catalysis • Copper catalysis • Ligand design • Silanol • N-H insertion

- [1] R. Noyori, *Angew. Chem. Int. Ed.* **2002**, *41*, 2008–2022.
- [2] A. Fanourakis, P. J. Docherty, P. Chuentragool, R. J. Phipps, *ACS Catal.* **2020**, *10*, 10672–10714.
- [3] D. W. C. MacMillan, *Nature* **2008**, *455*, 304–308.
- [4] R. Connon, B. Roche, B. V. Rokade, P. J. Guiry, *Chem. Rev.* **2021**, *121*, 6373–6521.
- [5] T. P. Yoon, E. N. Jacobsen, *Science* **2003**, *299*, 1691–1693.
- [6] J. F. Hartwig, *Nature* **2008**, *455*, 314–322.
- [7] J. Margalef, M. Biosca, P. de la Cruz Sánchez, J. Faiges, O. Pàmies, M. Diéguez, *Coord. Chem. Rev.* **2021**, *446*, 214120.
- [8] W. Zeng, G.-Y. Chen, Y.-G. Zhou, Y.-X. Li, *J. Am. Chem. Soc.* **2007**, *129*, 750–751.
- [9] A. Pfaltz, I. Drury, William J., *ChemInform* **2004**, *101*, 5723–5726.

- [10] G. Helmchen, A. Pfaltz, *Acc. Chem. Res.* **2000**, *33*, 336–345.
- [11] F. Menges, M. Neuburger, A. Pfaltz, *Org. Lett.* **2002**, *4*, 4713–4716.
- [12] M. J. Burk, *J. Am. Chem. Soc.* **1991**, *113*, 8518–8519.
- [13] H. Park, R. Kumareswaran, T. V. RajanBabu, *Tetrahedron* **2005**, *61*, 6352–6367.
- [14] B. L. Feringa, *Acc. Chem. Res.* **2000**, *33*, 346–353.
- [15] B. Bartels, G. Helmchen, *Chem. Commun.* **1999**, 741–742.
- [16] M. C. Schwarzer, A. Fujioka, T. Ishii, H. Ohmiya, S. Mori, M. Sawamura, *Chem. Sci.* **2018**, *9*, 3484–3493.
- [17] C. A. Krueger, K. W. Kuntz, C. D. Dzierba, W. G. Wirschun, J. D. Gleason, M. L. Snapper, A. H. Hoveyda, *J. Am. Chem. Soc.* **1999**, *121*, 4284–4285.
- [18] N. S. Josephsohn, K. W. Kuntz, M. L. Snapper, A. H. Hoveyda, *J. Am. Chem. Soc.* **2001**, *123*, 11594–11599.
- [19] A. Matsuzawa, T. Mashiko, N. Kumagai, M. Shibasaki, *Angew. Chem. Int. Ed.* **2011**, *50*, 7616–7619.
- [20] K. Narasaka, N. Iwasawa, M. Inoue, T. Yamada, M. Nakashima, J. Sugimori, *J. Am. Chem. Soc.* **1989**, *111*, 5340–5345.
- [21] E. J. Corey, Y. Matsumura, *Tetrahedron Lett.* **1991**, *32*, 6289–6292.
- [22] G. T. Notte, J. L. Leighton, *J. Am. Chem. Soc.* **2008**, *130*, 6676–6677.
- [23] Y. Sakaguchi, Y. Iwade, T. Sekikawa, T. Minami, Y. Hatanaka, *Chem. Commun.* **2013**, *49*, 11173.
- [24] K. Maruoka, H. Banno, H. Yamamoto, *J. Am. Chem. Soc.* **1990**, *112*, 7791–7793.
- [25] H. Zhang, D. Zhao, *ACS Catal.* **2021**, *11*, 10748–10753.
- [26] X. Chang, P. Ma, H. Chen, C. Li, P. Wang, *Angew. Chem. Int. Ed.* **2020**, *59*, 8937–8940.
- [27] H. F. Sore, W. R. J. D. Galloway, D. R. Spring, *Chem Soc Rev* **2012**, *41*, 1845–1866.
- [28] B. Yang, J. Gao, X. Tan, Y. Ge, C. He, *Angew. Chem. Int. Ed.* **2023**, e202307812.
- [29] P. Sangtrirugnul, T. D. Tilley, *Organometallics* **2007**, *26*, 5557–5568.
- [30] T. Kitano, T. Komuro, R. Ono, H. Tobita, *Organometallics* **2017**, *36*, 2710–2713.
- [31] Z. Mo, A. Kostenko, Y.-P. Zhou, S. Yao, M. Driess, *Chem. – Eur. J.* **2018**, *24*, 14608–14612.
- [32] T. Komuro, D. Mochizuki, H. Hashimoto, H. Tobita, *Dalton Trans.* **2022**, *51*, 9983–9987.
- [33] T. Komuro, Y. Nakajima, J. Takaya, H. Hashimoto, *Coord. Chem. Rev.* **2022**, *473*, 214837.
- [34] J. T. Poulton, M. P. Sigalas, K. Folting, W. E. Streib, O. Eisenstein, K. G. Caulton, *Inorg. Chem.* **1994**, *33*, 1476–1485.
- [35] M. H. Chisholm, F. A. Cotton, M. W. Extine, R. L. Kelly, *J. Am. Chem. Soc.* **1978**, *100*, 3354–3358.
- [36] A. Fürstner, *Angew. Chem. Int. Ed.* **2013**, *52*, 2794–2819.
- [37] J. Heppekausen, R. Stade, A. Kondoh, G. Seidel, R. Goddard, A. Fürstner, *Chem Eur J* **2012**, *18*, 10281–10299.
- [38] H. Yamagishi, J. Shimokawa, H. Yorimitsu, *ACS Catal.* **2023**, *13*, 7472–7487.
- [39] A. Fürstner, *J. Am. Chem. Soc.* **2021**, jacs.1c08040.
- [40] J. Hillenbrand, M. Leutzsch, E. Yiannakas, C. P. Gordon, C. Wille, N. Nöthling, C. Copéret, A. Fürstner, *J. Am. Chem. Soc.* **2020**, *142*, 11279–11294.
- [41] S. E. Denmark, R. C. Smith, *J. Am. Chem. Soc.* **2010**, *132*, 1243–1245.
- [42] S. E. Denmark, *J. Org. Chem.* **2009**, *74*, 2915–2927.
- [43] S. E. Denmark, A. Ambrosi, *Org. Process Res. Dev.* **2015**, *19*, 982–994.
- [44] S. A. Tymonko, R. C. Smith, A. Ambrosi, M. H. Ober, H. Wang, S. E. Denmark, *J. Am. Chem. Soc.* **2015**, *137*, 6200–6218.
- [45] C. Huang, B. Chattopadhyay, V. Gevorgyan, *J. Am. Chem. Soc.* **2011**, *133*, 12406–12409.
- [46] C. Huang, N. Ghavtadze, B. Chattopadhyay, V. Gevorgyan, *J. Am. Chem. Soc.* **2011**, *133*, 17630–17633.
- [47] C. Huang, N. Ghavtadze, B. Godoi, V. Gevorgyan, *Chem. – Eur. J.* **2012**, *18*, 9789–9792.
- [48] M. Parasram, V. Gevorgyan, *Acc. Chem. Res.* **2017**, *50*, 2038–2053.
- [49] S. M. Sieburth, L. Fensterbank, *J. Org. Chem.* **1993**, *58*, 6314–6318.
- [50] C. Golz, P. Steffen, C. Strohmman, *Angew. Chem. Int. Ed.* **2017**, *56*, 8295–8298.
- [51] F. Langenohl, J. Rösler, S. Zühlke, J. Kirchhoff, C. Strohmman, *Chem. – Eur. J.* **2023**, *29*, e202202935.
- [52] S. Özçubukçu, F. Schmidt, C. Bolm, *Org. Lett.* **2005**, *7*, 1407–1409.
- [53] C. C. Bausch, A. Pfaltz, *PHOX Ligands. In Privileged Chiral Ligands and Catalysts*, Wiley-VCH Verlag GmbH & Co. KGaA, **2011**.
- [54] G. C. Hargaden, P. J. Guiry, *Chem. Rev.* **2009**, *109*, 2505–2550.
- [55] G. Desimoni, G. Faita, K. A. Jørgensen, *Chem. Rev.* **2006**, *106*, 3561–3651.
- [56] S. O. Wilson, N. T. Tran, A. K. Franz, *Organometallics* **2012**, *31*, 6715–6718.
- [57] M. Jeon, J. Han, J. Park, *ACS Catal.* **2012**, *2*, 1539–1549.
- [58] L3a was found to be stable to air and atmospheric moisture for >30 months with minimal decomposition and no loss of catalytic activity., .
- [59] B. Liu, S.-F. Zhu, W. Zhang, C. Chen, Q.-L. Zhou, *J. Am. Chem. Soc.* **2007**, *129*, 5834–5835.
- [60] S.-F. Zhu, Q.-L. Zhou, *Acc. Chem. Res.* **2012**, *45*, 1365–1377.
- [61] L. G. Furniel, R. Echemendía, A. C. B. Burtoloso, *Chem. Sci.* **2021**, *12*, 7453–7459.
- [62] D. Gillingham, N. Fei, *Chem. Soc. Rev.* **2013**, *42*, 4918.
- [63] M.-L. Li, J.-H. Yu, Y.-H. Li, S.-F. Zhu, Q.-L. Zhou, *Science* **2019**, *366*, 990–994.
- [64] M.-L. Li, J.-B. Pan, Q.-L. Zhou, *Nat. Catal.* **2022**, *5*, 571–577.
- [65] Z. Liu, C. Calvó-Tusell, A. Z. Zhou, K. Chen, M. Garcia-Borràs, F. H. Arnold, *Nat. Chem.* **2021**, *13*, 1166–1172.
- [66] W. Yang, M. Pu, X. Lin, M. Chen, Y. Song, X. Liu, Y.-D. Wu, X. Feng, *J. Am. Chem. Soc.* **2021**, *143*, 9648–9656.
- [67] E. C. Lee, G. C. Fu, *J. Am. Chem. Soc.* **2007**, *129*, 12066–12067.
- [68] S.-F. Zhu, B. Xu, G.-P. Wang, Q.-L. Zhou, *J. Am. Chem. Soc.* **2012**, *134*, 436–442.
- [69] Y. Zhu, X. Liu, S. Dong, Y. Zhou, W. Li, L. Lin, X. Feng, *Angew. Chem. Int. Ed.* **2014**, *53*, 1636–1640.
- [70] The direct comparison ligand is to replace the diisopropylsilanol with diisopropylmethylsilyl; however, the ligand is not accessible. The trimethyl silyl group is the next best alternative for comparing silanol (L3g) and trialkylsilyl (L4), showing a decrease in selectivity from 56:44 er to 50:50 er.
- [71] No disiloxane formation was observed, and in one reaction under optimal conditions, L3a was successfully reisolated. The presence of the silanol ligand L3 was confirmed after each N–H insertion through <sup>19</sup>F NMR spectroscopy.
- [72] The reduced yield observed for 7b is attributed to the formation of side products, including carbene dimers and azines: Y. Li, Y.-T. Zhao, T. Zhou, M.-Q. Chen, Y.-P. Li, M.-Y. Huang, Z.-C. Xu, S.-F. Zhu, Q.-L. Zhou, *J. Am. Chem. Soc.* **2020**, *142*, 10557–10566.
- [73] W.-S. Huang, Z. Xu, K.-F. Yang, L. Chen, Z.-J. Zheng, L.-W. Xu, *RSC Adv.* **2015**, *5*, 46455–46463.
- [74] For substrates prone to β-H elimination, such as benzyl 5e and allyl 5f substrates, a consistent trend of higher yield was observed for the benzyl N-H insertion product: P. Guo, Y. Chen, L. Tao, S. Ji, R. Zhang, Z. Zhang, X. Liang, D. Wang, Y. Li, J. Zhao, *ACS Catal.* **2024**, *14*, 4690–4698.

- [75] Corwin. Hansch, A. Leo, R. W. Taft, *Chem. Rev.* **1991**, *91*, 165–195.
- [76] J.-B. Pan, X.-G. Zhang, Y.-F. Shi, A.-C. Han, Y.-J. Chen, J. Ouyang, M.-L. Li, Q.-L. Zhou, *Angew. Chem. Int. Ed.* **2023**, *62*, e202300691.
- [77] V. Dragojlovic, *ChemTexts* **2015**, *1*, 14.
- [78] K. B. Wiberg, *J. Org. Chem.* **2003**, *68*, 9322–9329.
- [79] L. Yao, K. Ishihara, *Chem. Sci.* **2019**, *10*, 2259–2263.
- [80] N. Smrečki, T. Rončević, O. Jović, B.-M. Kukovec, A. Maravić, G. Gajski, V. Čikeš-Čulić, *Inorganica Chim. Acta* **2019**, *488*, 312–320.
- [81] N. Pantalon Juraj, T. Tandarić, V. Tadić, B. Perić, D. Moreth, U. Schatzschneider, A. Brozovic, R. Vianello, S. I. Kirin, *Dalton Trans.* **2022**, *51*, 17008–17021.
- [82] J. C. Slootweg, P. Chen, *Organometallics* **2006**, *25*, 5863–5869.
- [83] E. Iniesta, A. Vidal-Ferran, *Chem. Commun.* **2020**, *56*, 6364–6367.
- [84] Deposition numbers 2289933 (for **L3a**), 2289935 (for **L3b**), 2289936 (for **3a**), 2289938 (for **S2**), 2289939 (for **L1a**), and 2311643 (for  $[(\mathbf{L3a})_2\mathbf{Na}\cdot(\mathbf{H}_2\mathbf{O})_2]^+\mathbf{[BAR}^f\mathbf{]}^-$ ) contain the supplementary crystallographic data for this paper. These data are provided free of charge by the joint Cambridge Crystallographic Data Centre and Fachinformationszentrum Karlsruhe Access Structures service.